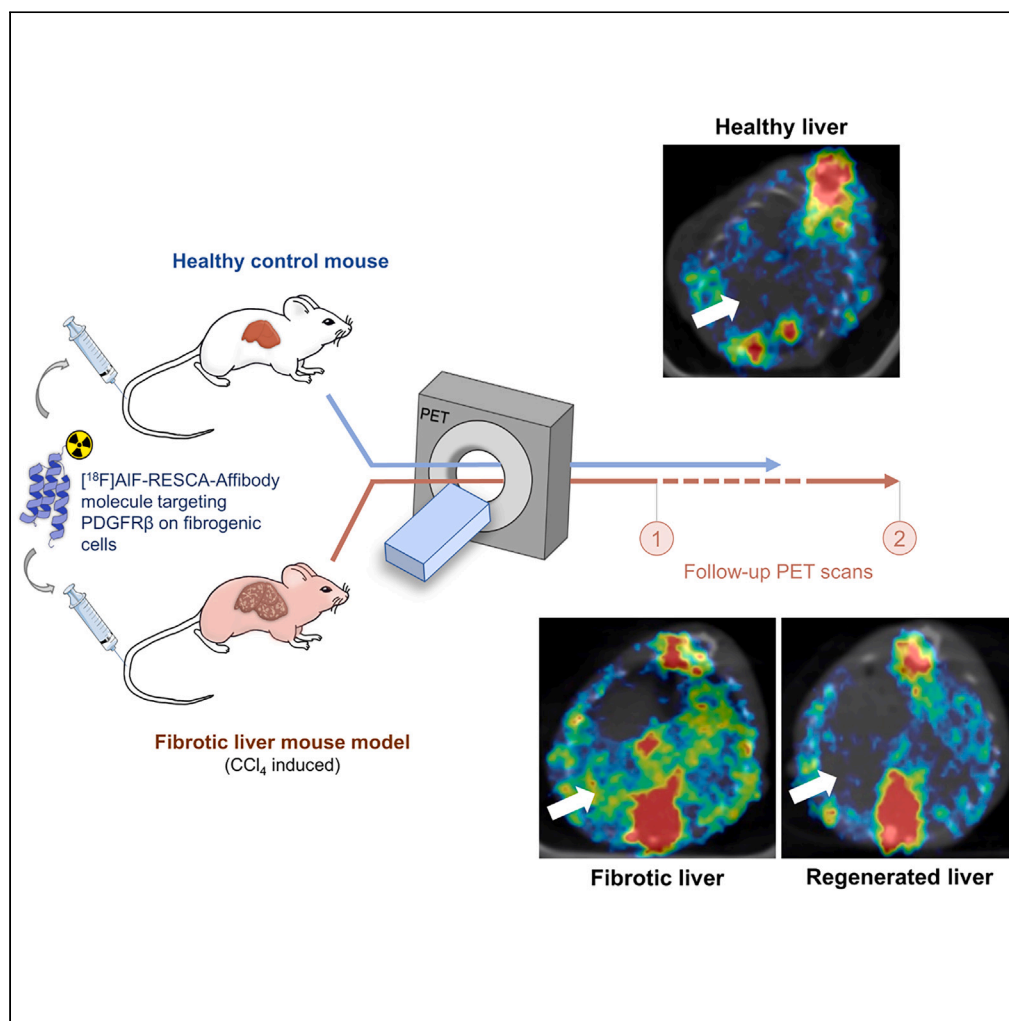


## Article

## Non-invasive PET imaging of liver fibrogenesis using a RESCA-conjugated Affibody molecule



Olivia Wegrzyniak,  
Francesco Lechi,  
Bogdan Mitran, ...,  
Olle Korsgren, Bo  
Zhang, Olof  
Eriksson

olof.eriksson@ilk.uu.se

**Highlights**

PDGFR $\beta$  PET imaging is an  
NIT characterizing  
fibrogenic cells

Liver tracer uptake  
decreased during  
regeneration versus severe  
fibrosis in mice

PDGFR $\beta$  PET scan may  
offer a responsive readout  
of antifibrotic candidate  
drug activity

Wegrzyniak et al., iScience 27,  
109688

May 17, 2024 © 2024 The  
Authors. Published by Elsevier  
Inc.

[https://doi.org/10.1016/  
j.isci.2024.109688](https://doi.org/10.1016/j.isci.2024.109688)

## Article

## Non-invasive PET imaging of liver fibrogenesis using a RESCA-conjugated Affibody molecule

Olivia Wegrzyniak,<sup>1</sup> Francesco Lechi,<sup>1</sup> Bogdan Mitran,<sup>1,2</sup> Pierre Cheung,<sup>1</sup> Athanasios Bitzios,<sup>1</sup> Jonas Persson,<sup>1,3</sup> John Löfblom,<sup>3</sup> Helena Nordström,<sup>4</sup> Jonas Eriksson,<sup>1,5</sup> Fredrik Y. Frejd,<sup>6,7</sup> Olle Korsgren,<sup>6</sup> Bo Zhang,<sup>1</sup> and Olof Eriksson<sup>1,2,8,\*</sup>

## SUMMARY

**Non-invasive assessment of fibrogenic activity, rather than fibrotic scars, could significantly improve the management of fibrotic diseases and the development of anti-fibrotic drugs. This study explores the potential of an Affibody molecule (Z09591) labeled with the Al(18)F-restrained complexing agent (RESCA) method as a tracer for the non-invasive detection of fibrogenic cells. Z09591 was functionalized with the RESCA chelator for direct labeling with [<sup>18</sup>F]AIF. *In vivo* positron emission tomography/magnetic resonance imaging scans on U-87 tumor-bearing mice exhibited high selectivity of the resulting radiotracer, [<sup>18</sup>F]AIF-RESCA-Z09591, for platelet-derived growth factor receptor  $\beta$  (PDGFR $\beta$ ), with minimal non-specific background uptake. Evaluation in a mouse model with carbon tetrachloride-induced fibrotic liver followed by a disease regression phase, revealed the radiotracer's high affinity and specificity for fibrogenic cells in fibrotic livers (standardized uptake value [SUV]  $0.43 \pm 0.05$ ), with uptake decreasing during recovery (SUV  $0.29 \pm 0.03$ ) ( $p < 0.0001$ ). [<sup>18</sup>F]AIF-RESCA-Z09591 accurately detects PDGFR $\beta$ , offering non-invasive assessment of fibrogenic cells and promising applications in precise liver fibrogenesis diagnosis, potentially contributing significantly to anti-fibrotic drug development.**

## INTRODUCTION

Fibrosis is characterized as an abnormal wound-healing response that can ultimately result in organ failure. Fibrosis is present in a variety of pathologies that affect a wide range of organs, including chronic liver diseases (CLDs), myocardial infarction, and interstitial lung disease.<sup>1</sup> As a result, the incidence of fibrosis and related pathologies is significant.

However, there is a lack of effective anti-fibrotic treatments. This can be partially explained by the lack of suitable techniques to monitor early responses to treatment.<sup>2,3</sup> Current fibrosis assessment relies on invasive techniques, such as biopsies, which pose challenges in terms of scalability due to the associated risks involved in these interventions.<sup>4</sup> Given the inherent limitations of liver biopsies, it has become essential to clinically adopt non-invasive methods for assessing liver fibrosis. Imaging techniques such as magnetic resonance (MR) and ultrasound elastography, as well as computed tomography (CT)-based methods, have gained prominence. However, these non-invasive techniques (NITs), while providing valuable alternatives, are constrained by their low sensitivity, particularly in the early detection of diseases.<sup>3</sup> Furthermore, there are currently no NITs clinically available that can effectively differentiate between active fibrogenesis and stable scars.

Platelet-derived growth factor receptor  $\beta$  (PDGFR $\beta$ ) is a biomarker of pericytes, and in the context of liver fibrosis, activated hepatic stellate cells (aHSC),<sup>5,6</sup> which play a crucial role in the deposition of extracellular matrix (ECM).<sup>7</sup> Previously, an Affibody molecule (Z09591) with a sub-nanomolar affinity for PDGFR $\beta$  was radiolabeled by a prosthetic fluorine-18 labeled tetrazine (TZ) group. [<sup>18</sup>F]TZ-Z09591 allowed the *in vivo* assessment of fibrogenic cells in a murine model of acute liver fibrosis.<sup>8</sup>

The Al(18)F-restrained complexing agent (RESCA) method is a chelator-based radiolabeling method.<sup>9</sup> It enables the convenient radiolabeling of a molecule containing a RESCA chelator with fluorine-18. This <sup>18</sup>F labeling process can be completed quickly and in a single step under mild conditions, adhering to good manufacturing practices. <sup>18</sup>F radiolabeled positron emission tomography (PET) tracers are preferred for PET imaging because of their lower positron energy (0.65 vs. 1.90 MeV), which results in improved spatial resolution. Additionally, the

<sup>1</sup>Science for Life Laboratory, Department of Medicinal Chemistry, Uppsala University, Uppsala, Sweden

<sup>2</sup>Antaros Medical AB, Mölndal, Sweden

<sup>3</sup>Department of Protein Science, Division of Protein Engineering, KTH Royal Institute of Technology, Stockholm, Sweden

<sup>4</sup>Science for Life Laboratory, Drug Discovery & Development Platform, Department of Chemistry-BMC, Uppsala University, Uppsala, Sweden

<sup>5</sup>PET Center, Uppsala University Hospital, Uppsala, Sweden

<sup>6</sup>Department of Immunology, Genetics and Pathology, Uppsala University, Uppsala, Sweden

<sup>7</sup>Affibody AB, Solna, Sweden

<sup>8</sup>Lead contact

\*Correspondence: [olof.eriksson@ilk.uu.se](mailto:olof.eriksson@ilk.uu.se)

<https://doi.org/10.1016/j.isci.2024.109688>



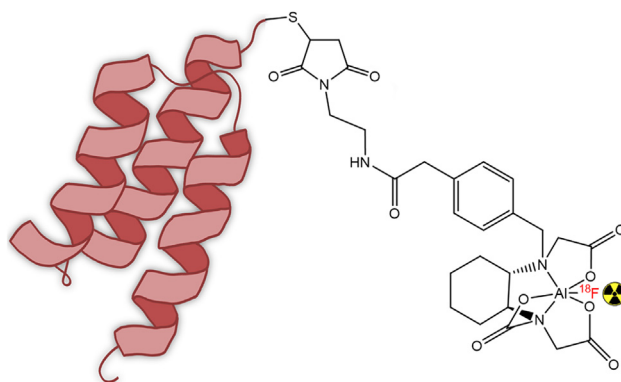


**Figure 1.  $[^{18}\text{F}]\text{AIF-RESCA-Z09591}$  structure**

Schematic presentation of the molecular structure of the conjugated radiotracer  $[^{18}\text{F}]\text{AIF-RESCA-Z09591}$ .

longer physical half-life (110 min) facilitates off-site production of high activities for convenient shipment, offering operational advantages and clinical adaptability.

Therefore, considering the significance of PDGFR $\beta$  in the fibrogenesis process, the high affinity of Z09591 to this biomarker, and the properties of the Al(18)F-RESCA labeling, it was hypothesized that  $[^{18}\text{F}]\text{AIF-RESCA-Z09591}$  (Figure 1) could serve as a PET tracer for imaging the changes in fibrosis level in tissue. To investigate the aforementioned hypothesis, *in vivo* evaluation of  $[^{18}\text{F}]\text{AIF-RESCA-Z09591}$  was conducted, focusing on a carbon tetrachloride ( $\text{CCl}_4$ )-induced model of fibrosis, both during the progression and regression phases of liver fibrotic pathology.

## RESULTS

### *In vitro* characterization

The equilibrium dissociation constant ( $K_D$ ) for human PDGFR $\beta$  was  $0.33 \pm 0.03$  nM (Figure 2A) (Table S3), while for murine PDGFR $\beta$  it was  $2.4 \pm 0.5$  nM (Figure 2B) (Table S4). No measurable interaction was observed with human PDGFR $\alpha$  at the concentrations tested (up to  $3 \mu\text{M}$ ) (Figure S2). The *in vitro* specificity was assessed using cell binding assays with autoradiography (ARG) on U-87 and K-562 cells, which demonstrated that the uptake of the radiotracer was high in U-87 cell pellets ( $29.05 \pm 2.24$  fmol/ $\text{mm}^3$ ) compared to K-562 cell pellets ( $0.97 \pm 0.21$  fmol/ $\text{mm}^3$ ), and significantly reduced in U-87 cells pre-incubated with Cys-Z09591 ( $4.74 \pm 0.91$  fmol/ $\text{mm}^3$ ) (Figures 2C–2E). The *in vitro* ARG performed on a liver fibrosis biopsy from a patient demonstrated that when incubated with the radiotracer alone, there was a strong and heterogeneous uptake in fibrous septa. The uptake was not observed in the biopsy incubated with Cys-Z09591. The uptake of radioactivity correlated with collagen deposition and PDGFR $\beta$  expression, as demonstrated by Sirius red (SIR) and PDGFR $\beta$  immunohistochemistry (IHC) stainings, respectively (Figure 2F).

### Dosimetry in rat and pig

A whole-body PET/CT scan was conducted on healthy rats and pig to study the pharmacokinetics of  $[^{18}\text{F}]\text{AIF-RESCA-Z09591}$ . The tracer exhibited fast blood clearance (Figures S3 and S5). Excretion occurred through the kidneys, resulting in an increased renal uptake in rats and pig after 1 h. The background uptake in several tissues commonly affected by fibrosis, such as the liver and lung, decreased over time. The  $\text{SUV}_{\text{mean}}$  in the liver was below 1.3 after 30 min, below 0.8 after 1 h, and finally below 0.4 after 2 h in rats and pig. All  $\text{SUV}_{\text{mean}}$  values from other organs were below one after 40 min and decreased over time in pig. Similar results were observed in rats, except in bone with a  $\text{SUV}_{\text{mean}}$  above 2 after 2 h, while it was 0.41 for the pig.  $[^{18}\text{F}]\text{AIF-RESCA-Z09591}$  demonstrated high *in vivo* stability in pig plasma, with over 95% remaining intact for up to 60 min after administration (Figure S4; Table S5).

The predicted human dosimetry was extrapolated from the *ex vivo* biodistribution data in rats and pig (Table S6). The effective dose of  $[^{18}\text{F}]\text{AIF-RESCA-Z09591}$  for human males was calculated to be 0.020 mSv/MBq and 0.007 mSv/MBq, extrapolated from rats and pig, respectively.

### *In vivo* evaluation in a U-87 xenograft model

The use of  $[^{18}\text{F}]\text{AIF-RESCA-Z09591}$  as a PET tracer enabled clear visualization of PDGFR $\beta$  expression in U-87 xenografts. This uptake was not observed in the blocking condition (Figure 3A). The *in vivo* biodistribution study demonstrated that the tumor uptake was higher than in other organs, except for the kidneys (Figure 3B). The uptake of  $[^{18}\text{F}]\text{AIF-RESCA-Z09591}$  in tumors in the non-blocked condition was significantly higher compared to tumors from mice in the blocking condition ( $\text{SUV } 0.733 \pm 0.15$  and  $0.12 \pm 0.03$ , respectively) (Figure 3C). The same observation can be made in the spleen, where the uptake can be blocked. In the murine spleen, PDGFR $\beta$  is expressed (Figure S6). The uptake in bone ( $\text{SUV } 0.37 \pm 0.04$ ) was elevated compared to blood ( $\text{SUV } 0.11 \pm 0.01$ ), suggesting a degree of de-fluorination and the subsequent binding of free fluorine-18 with apatite in bone tissue.

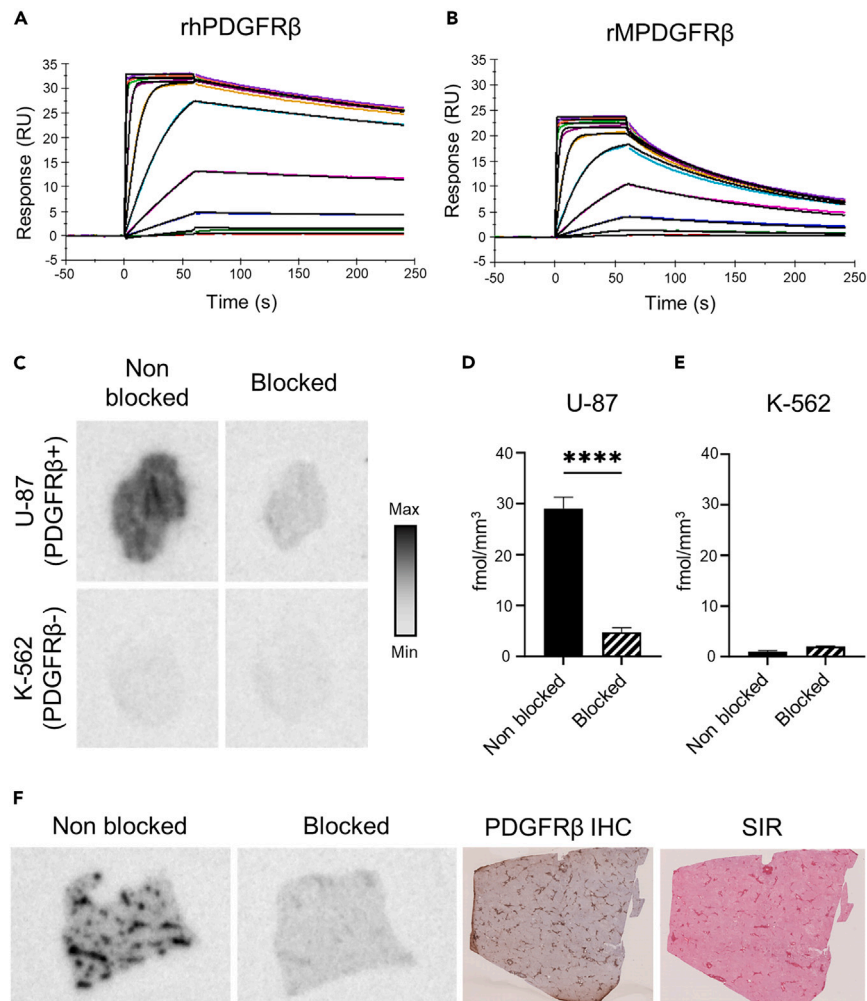


**Figure 2. In vitro evaluation of  $[^{18}\text{F}]\text{AIF-RESCA-Z09591}$**

(A and B) Sensogram plots generated by SPR kinetic analysis demonstrate the association and dissociation characteristics between RESCA-Z09591 immobilized (A) rhPDGFR $\beta$  and (B) rMPDGFR $\beta$ .

(C–E) (C) ARG of  $[^{18}\text{F}]\text{AIF-RESCA-Z09591}$ , (D) mean tracer uptake of U-87 cells (expressing PDGFR $\beta$ ), and (E) K-562 cells (no PDGFR $\beta$  expression) in non-blocked ( $n = 4$  and  $n = 2$ , for U-87 and K-562, respectively) or blocked condition ( $n = 4$  and  $n = 2$ , for U-87 and K-562, respectively) (bars represent SD). In (D) levels of significance: \*\*\*\* $p \leq 0.0001$  (unpaired t test, see details in Table S7).

(F) ARG of  $[^{18}\text{F}]\text{AIF-RESCA-Z09591}$ , PDGFR $\beta$  immunostaining (PDGFR $\beta$  in brown), and SIR (collagen fibers in red) staining on a human fibrotic liver. IHC, immunohistochemistry; RU, resonance units; SIR, Sirius red.

### Liver fibrosis model

$[^{18}\text{F}]\text{AIF-RESCA-Z09591}$  PET/CT scans revealed that the SUV in fibrotic livers of mice treated with  $\text{CCl}_4$  was higher than that in healthy livers, and this uptake was reduced under blocking conditions (Figure 4A). These observations are consistent with the ex vivo biodistribution and ARG. Ex vivo biodistribution results from livers showed that the SUV in the livers of  $\text{CCl}_4$  mice ( $0.43 \pm 0.05$ ) was significantly higher than that in the livers of healthy mice ( $0.24 \pm 0.03$ ). The uptake in the fibrotic liver significantly decreased when the target was saturated with Cys-Z09591 ( $0.27 \pm 0.024$ ) (Figure 4C). No difference was observed in the healthy livers of mice under non-blocking or blocking conditions. Ex vivo ARGs exhibited similar results, with strong heterogeneous uptake observed only in the fibrotic liver (Figure 4D). This uptake corresponded to collagen deposition and PDGFR $\beta$  expression, as demonstrated by SIR (staining collagen fibers) and PDGFR $\beta$  IHC stainings, respectively (Figure S8). The details of the staining performance are described in the supplemental information. This uptake was not observed in healthy livers or in livers from  $\text{CCl}_4$ -treated mice injected with Cys-Z09591. In both healthy and  $\text{CCl}_4$  mice, tracer uptake was observed in the spleens, and it was decreased under blocking conditions (Figures 4D and S7). Similar to the results obtained in the U-87 xenograft model, the uptake in bone was also higher compared to that in the blood.

The toxicity of  $\text{CCl}_4$  leading to fibrosis in mice after six weeks of treatment was also observed by electron microscopy. Changes in tissue architecture were observed in the liver of  $\text{CCl}_4$ -treated mice, specifically hepatocellular ballooning degeneration. This was characterized by

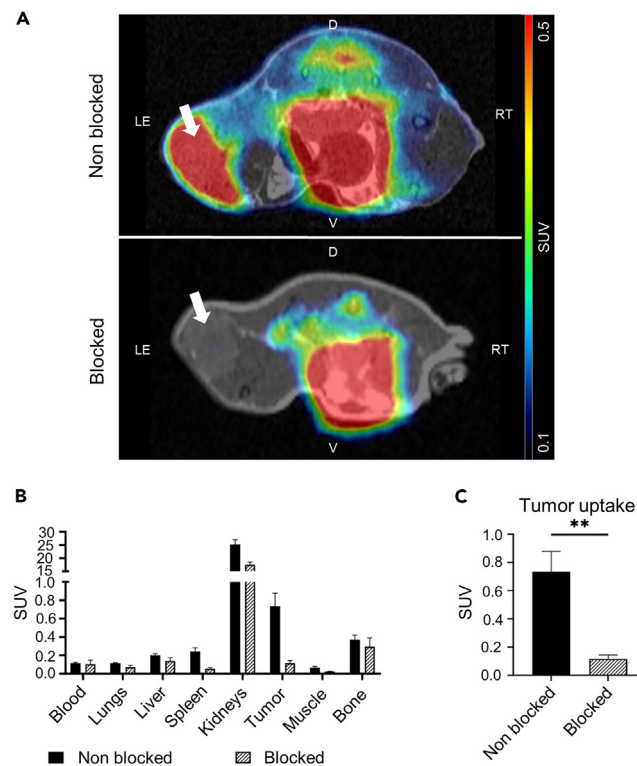


**Figure 3. PET/MRI images and ex vivo biodistribution of xenograft mice**

(A) Comparison of [<sup>18</sup>F]AIF-RESCA-Z09591 PET/MRI images (transverse sections) 60 min post-injection.

(B) Mean [<sup>18</sup>F]AIF-RESCA-Z09591 uptake in organs of interest.

(C) Mean tumor uptake in non-blocked (n = 4) and blocked condition (n = 4) (bars represent SD). Levels of significance: \*\*p = 0.0028 (Welch's t test, see details in Table S8). The white arrows indicate the tumor. D, dorsal; LE, left; Mu, muscle; RT, right; Sp, spleen; SUV, standardized uptake value; Tu, tumor; V, ventral.

swollen hepatocytes with rarified cytoplasm (Figure S11), resulting in a significantly enlarged liver in CCl<sub>4</sub>-treated mice compared to the control (Figure S10B).

To study fibrogenesis and regression, follow-up PET/CT scans were conducted on mice treated with CCl<sub>4</sub> at the peak of the disease and one to two weeks into regression. After one week of regression, there was no noticeable decrease in liver uptake (Figures S9A and S10A). However, tracer uptake tended to be higher in other organs, such as the lungs, muscles, and blood (Figure S10C). The variations in protein dosage injected, caused by differences in the RCY, might explain the lack of reduction in liver uptake despite decreased PDGFRβ levels after one week of regression (Figures S9B and S12). After two weeks of regression, the liver uptake significantly decreased (Figures 4B and 4C). The ex vivo biodistribution (Figure 4C) was consistent with the PET/CT results (Figure 4B). Two weeks after completion of the six weeks CCl<sub>4</sub> treatment, the uptake of [<sup>18</sup>F]AIF-RESCA-Z09591 in the liver was significantly reduced compared to the peak of the disease (SUV 0.43 ± 0.05, and 0.29 ± 0.03, respectively) and almost normalized to that of a healthy liver (SUV 0.24 ± 0.03). Histological analysis revealed a decrease in collagen deposition and PDGFRβ expression (Figure S12) overtime during the regression phase, reaching a level similar to those in the healthy liver after two weeks of regression. However, regenerating livers remained larger and more swollen than healthy livers (Figure S10B).

## DISCUSSION

A NIT that enables the visualization and quantification of fibrogenesis would be extremely valuable for developing new anti-fibrotic therapies and improving disease management by enabling early diagnosis and precise staging of fibrosis. PET scans, exemplified by [<sup>18</sup>F]FDG, have been investigated as a NIT for assessing liver fibrosis. However, the inherent lack of specificity in [<sup>18</sup>F]FDG, which primarily reflects glucose use, poses challenges due to potential influences from factors unrelated to fibrogenesis. [<sup>18</sup>F]FDG uptake was observed in both the steatosis<sup>10,11</sup> and fibrosis<sup>12</sup> stages, indicating that its uptake does not appear to be specific to fibrosis. To address these limitations, our approach involves imaging a receptor that is selectively expressed on the surface of fibrogenic cells to achieve a more precise and specific assessment of fibrogenesis. PDGFRβ is a biomarker for liver fibrogenic cells, specifically aHSCs.<sup>5,7</sup> Liver fibrosis is a complex and dynamic process characterized by the activation of hepatic stellate cells (HSCs). During the regression phase, aHSCs exhibit a rapid decrease in their population,<sup>13</sup> in contrast to fibrous scars, which can take several years to resolve. Therefore, PDGFRβ is an interesting biomarker for characterizing fibrogenic activity. The PET tracer [<sup>18</sup>F]AIF-RESCA-Z09591, targeting PDGFRβ, was assessed for its capability to visualize fibrogenic cells in a dynamic model of liver fibrosis with spontaneous recovery.

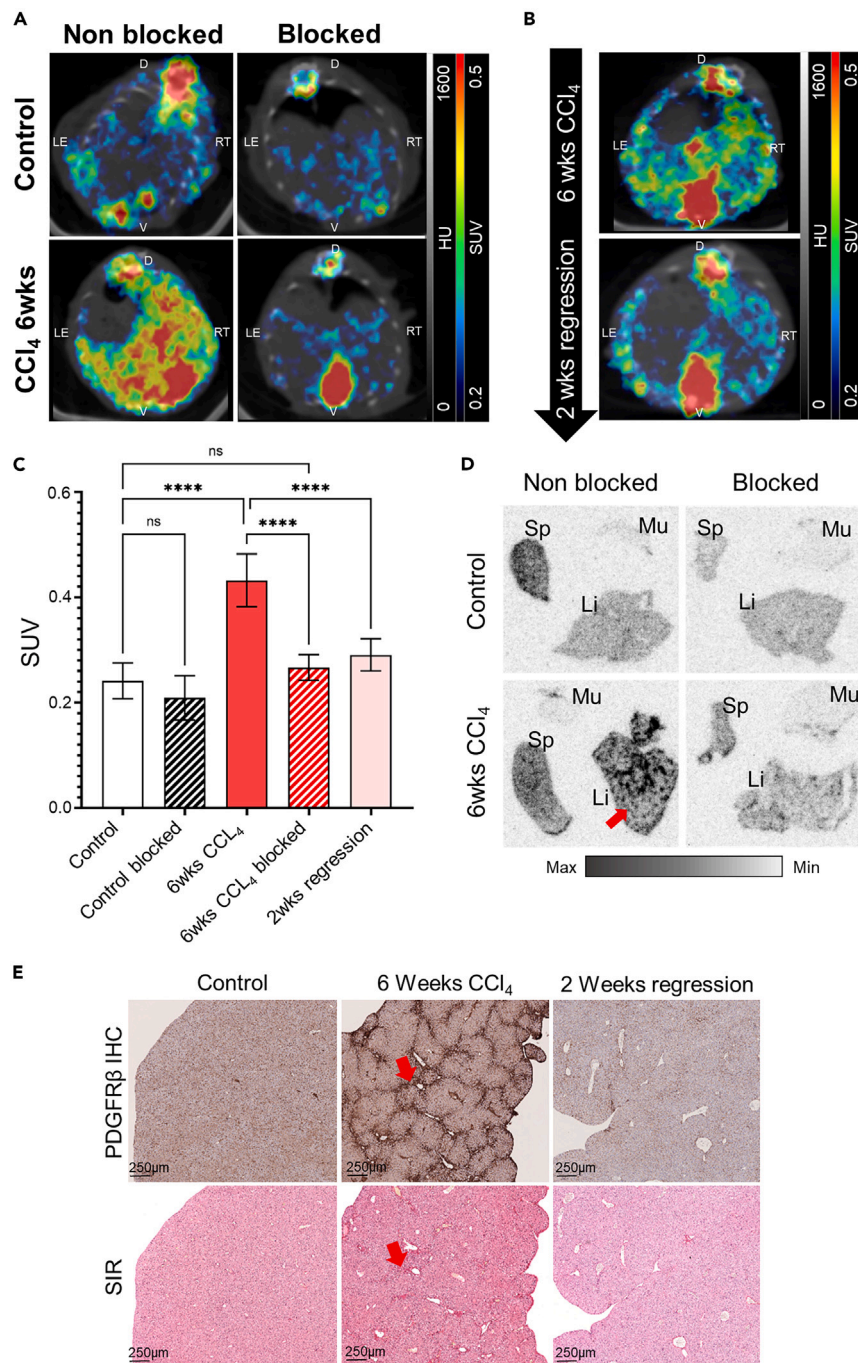


**Figure 4. Assessment of liver fibrogenesis in mice**

(A) PET/CT (transverse sections) 60 min post-injection (*p-i*) and *postmortem* in healthy control mice and CCl<sub>4</sub> mice in non-blocking or blocking condition.

(B) Follow-up PET/CT (transverse sections) 60 min *p-i* and *postmortem* in a single mouse from the end of the six weeks of CCl<sub>4</sub> treatment (6 weeks CCl<sub>4</sub>) to two weeks of regression (2 weeks regression).

(C) Mean [<sup>18</sup>F]AIF-RESCA-Z09591 uptake (from the *ex vivo* biodistribution) in the liver of control and CCl<sub>4</sub> mice in non-blocked and blocked condition, and after two weeks of liver regeneration (bars represent SD). Level of significance: \*\*\**p* ≤ 0.001. \*\*\*\**p* ≤ 0.0001 (ANOVA and Tukey's post-hoc tests, see details in Table S9).

(D) *Ex vivo* ARG of [<sup>18</sup>F]AIF-RESCA-Z09591 binding, in the liver (Li), muscle (Mu), and spleen (Sp), pretreated or not with Cys-Z09591.

(E) SIR (collagen fibers in red) and PDGFRβ immuno-histochemistry (PDGFRβ in brown) staining of liver from CCl<sub>4</sub> treated and healthy control mice (20.0× magnification). The red arrows indicate fibrous septa. D, dorsal; HU, Hounsfield units; IHC, immunohistochemistry; LE, left; RT, right; SIR, Sirius red; SUV, standardized uptake value, V, ventral.

The Affibody molecule Z09591 was previously labeled with a fluorine-18 labeled TZ group. [ $^{18}\text{F}$ ]TZ-Z09591 efficiently detected fibrogenic cells in the acute phase of liver fibrosis in  $\text{CCl}_4$  mice *in vivo*.<sup>8</sup> A new approach was employed to radiolabel the Affibody molecule Z09591 in this study. Specifically, the coordination of [ $^{18}\text{F}$ ]AIF to the chelator RESCA. The RESCA conjugation of Z09591 allows for easy radiolabeling with fluorine-18. This labeling method can be readily implemented at production sites and has a radioactive half-life that is long enough to enable the scanning of multiple patients during the course of a day, or transportation to remote PET sites from a central radiochemistry lab with cyclotron access. The AIF-RESCA method, which relies on basic bench chemistry, is a promising candidate for the automation of PET radiotracer labeling. This could improve radiochemical yields and synthesis consistency while concurrently reducing operator radiation exposure compared to manual labeling. Radiotracers labeled using this method were recently clinically evaluated and demonstrated favorable imaging characteristics in breast cancer patients.<sup>14,15</sup> RESCA conjugation to Z09591 did not affect the binding capacity of the Affibody molecule and retained picomolar and nanomolar affinities for PDGFR $\beta$  (Figures 2A and 2B; Tables S3 and S4), similar to the binding interactions previously observed using TCO-Z09591.<sup>8</sup> RESCA-Z09591 was successfully radiolabeled to [ $^{18}\text{F}$ ]AIF, and [ $^{18}\text{F}$ ]AIF-RESCA-Z09591 demonstrated *in vitro* and *in vivo* specificity toward U-87 cells expressing PDGFR $\beta$ .

[ $^{18}\text{F}$ ]AIF-RESCA-Z09591 demonstrated favorable pharmacokinetics for PET imaging (Figures S3 and S5). This radiotracer, in comparison to [ $^{18}\text{F}$ ]TZ-Z09591, exhibited lower background uptake in most organs, including the liver, which could allow for better visualization of liver fibrogenesis. Nevertheless, a significant and consistent uptake was observed in the kidneys, suggesting that the main pathway for the elimination the radioactivity is through renal excretion. This finding is regrettable, considering that PDGFR $\beta$  has been shown to play a significant role in renal fibrogenesis.<sup>16–18</sup> However, if the current molecular design of [ $^{18}\text{F}$ ]AIF-RESCA-Z09591 may not be suitable to image renal fibrosis, it may be theoretically possible to achieve decreased renal retention of Z09591 by using alternative radiolabeling strategies or cleavable linkers. However, it is important to consider that these approaches may also result in an increase in hepatic excretion and background levels. Furthermore, there was a relatively high uptake in bones compared to the blood in the murine models studied (ratio SUV<sub>bone/blood</sub> 3.30 and 0.93 for mice and pig, respectively). Biomolecules labeled with [ $^{18}\text{F}$ ]AIF-RESCA have previously demonstrated increased uptake in bone over time in murine models, which may indicate demetallation and/or defluorination of the compound.<sup>9</sup> [ $^{18}\text{F}$ ]AIF-RESCA-Z09591 exhibited a high stability in pig plasma at 15 min and up to 1 h post-injection (p-i) (Figure S4; Table S5), indicating low defluorination in pig. From these observations, it could be suggested that the phenomenon of bone uptake and defluorination of [ $^{18}\text{F}$ ]AIF-RESCA-Z09591 is mainly observed in murine models. Furthermore, a recent clinical study has been conducted to investigate the use of an [ $^{18}\text{F}$ ]AIF-RESCA labeled nanobody, [ $^{18}\text{F}$ ]AIF-RESCA-MIRC213, for imaging HER2-positive cancers through PET/CT. This study demonstrated that no significant radioactivity was detected in the bones of patients and that the use of the [ $^{18}\text{F}$ ]AIF-RESCA labeled molecule as a PET tracer was safe.<sup>14</sup> However, caution is necessary due to the limited observations in a single pig, and further studies on larger mammals are essential to make conclusive assessments regarding the risk of [ $^{18}\text{F}$ ]AIF-RESCA-Z09591 defluorination. The human dosimetry extrapolated from pig and rat biodistribution demonstrates that [ $^{18}\text{F}$ ]AIF-RESCA-Z09591 can be used for repeated scanning.

The ARG conducted on fibrotic human liver revealed a strong heterogeneous uptake in fibrous septa surrounding cirrhotic nodules (Figure 2E). This specific uptake observed in the human fibrotic liver underscores its potential for translational application in imaging liver fibrosis. [ $^{18}\text{F}$ ]AIF-RESCA-Z09591 also enabled the visualization of PDGFR $\beta$  expression in the fibrotic livers of mice treated with  $\text{CCl}_4$  (Figure 4). The results are correlated with the evaluation of [ $^{18}\text{F}$ ]TZ-Z09591 in  $\text{CCl}_4$  mice.<sup>8</sup> The uptake in fibrotic liver is linked with the expression of PDGFR $\beta$  on the surface of active fibrogenic cells located in areas with high remodeling activity, such as fibrous septa. During liver regeneration, the number of fibrogenic cells decreases as aHSCs are either deactivated<sup>19</sup> or eliminated,<sup>13,20</sup> resulting in reduced expression of PDGFR $\beta$ . This suggests that PDGFR $\beta$  is a potential suitable target for molecular imaging of fibrogenesis, and that [ $^{18}\text{F}$ ]AIF-RESCA-Z09591 has favorable characteristics for high-contrast PET images of active fibrogenic processes.

Additionally, fibrogenesis pathways are present in various fibrotic diseases, notably the platelet-derived growth factor (PDGF) signaling, which plays a central role in fibrogenesis.<sup>21–23</sup> [ $^{18}\text{F}$ ]AIF-RESCA-Z09591 PET could be an effective non-invasive method for imaging active fibrogenesis not only in the liver but also in other organs affected by fibrosis, even at an early stage. As a result, it could be used for early diagnosis, staging the severity of fibrotic diseases, monitoring disease progression, and even assessing regression following interventions.

[ $^{18}\text{F}$ ]AIF-RESCA-Z09591 possesses numerous advantages for clinical application in non-invasive visualization of fibrogenesis. This could benefit the significant global population affected by CLD.<sup>24</sup> Within CLDs, metabolic dysfunction-associated fatty liver disease (MAFLD), previously known as non-alcoholic fatty liver disease (NAFLD), has emerged as the most prevalent type.<sup>25</sup> With the rising prevalence of obesity<sup>26</sup> and type 2 diabetes,<sup>27</sup> the number of patients suffering from CLDs will continue to increase alarmingly. The chronic and long-term nature of MAFLD, along with its numerous associated comorbidities and consequent high costs, pose significant healthcare and socioeconomic challenges. Furthermore, the lack of effective anti-fibrotic therapies worsens these challenges. In 2017, the estimated lifetime cost of care for all patients with MAFLD in the US was \$222 billion.<sup>28</sup> As the prevalence of MAFLD increases, the associated healthcare costs will also increase. Therefore, it is crucial to mobilize efforts to improve the management of patients with CLDs. PET scans and the radiotracer [ $^{18}\text{F}$ ]AIF-RESCA-Z09591, described in this paper, align with this drive for improvement.

In conclusion, the PET tracer [ $^{18}\text{F}$ ]AIF-RESCA-Z09591 has the ability to evaluate changes in liver fibrosis by visualizing PDGFR $\beta$  expression on the surface of fibrogenic cells, indicating its potential for imaging of fibrogenesis. This PET radiotracer is suitable for conducting longitudinal studies to monitor disease progression in patients. This technique holds great promise in improving fibrosis management and the development of anti-fibrotic medications.

### Limitations of the study

The selection of the CCl<sub>4</sub> mice model as a preclinical representation of liver fibrosis introduces limitations to the study. This model, reliant on the injection of a toxic agent, offers the advantage of inducing rapid and reproducible severe liver fibrosis. However, the severity of this model can result in significant side effects, leading animals to reach the humane endpoint before the completion of the six-week CCl<sub>4</sub> treatment period. Notably, 31% of treated mice in this study reached the humane endpoint before the treatment conclusion. Furthermore, the CCl<sub>4</sub> model does not accurately replicate the pathogenesis and regression of the human disease. Unlike human liver fibrosis, where the resolution of fibrotic scars can take years, the mouse model exhibited scar reduction as early as one to two weeks of regression, complicating the distinction between fibrosis and fibrogenesis during the regression phase. However, PDGFR $\beta$  is a well-established fibrogenesis marker.<sup>5,6</sup> This marker is expressed on fibrogenic cells, known to diminish during liver regeneration,<sup>13,19,20</sup> in contrast to fibrotic scars. Thus, it is expected that assessing PDGFR $\beta$  corresponds to the evaluation of fibrogenesis rather than fibrosis. In addition, it is crucial to note that the affinity of the tracer for murine PDGFR $\beta$  is considerably lower, approximately ten times, than its affinity for human PDGFR $\beta$ . This discrepancy implies that the observations made on the mouse model may underestimate the true potential of the radiotracer. Finally, all CCl<sub>4</sub> mice in this study were female; therefore, the potential influence of sex on the results was not investigated.

### STAR★METHODS

Detailed methods are provided in the online version of this paper and include the following:

- KEY RESOURCES TABLE
- RESOURCE AVAILABILITY
  - Lead contact
  - Materials availability
  - Data and code availability
- EXPERIMENTAL MODEL AND STUDY PARTICIPANT DETAILS
  - Cell lines
  - Human liver biopsy
  - Animal models
- METHOD DETAILS
  - RESCA-Z09591 Affibody molecule production
  - Radiolabeling of RESCA-Z09591
  - *In vitro* studies
  - *In vivo* studies
- QUANTIFICATION AND STATISTICAL ANALYSIS

### SUPPLEMENTAL INFORMATION

Supplemental information can be found online at <https://doi.org/10.1016/j.isci.2024.109688>.

### ACKNOWLEDGMENTS

The RESCA-Z09591 Affibody molecule was provided by Affibody AB. The study was supported by an EFSD grant, Magnus Bergvalls Foundation, the Swedish Research Council (2020–02312), Barndiabetesfonden, Diabetesfonden, Diabetes Wellness and Science for Life Laboratory. The corelab staff at Preclinical PET/MRI Platform (PPP), Hedenstierna laboratory and the BioVis corelab at Uppsala University, as well as the Biophysical Screening and Characterization platform at SciLifeLab are acknowledged for technical assistance.

### AUTHOR CONTRIBUTIONS

O.W. researched, analyzed, interpreted data, and wrote the manuscript. F.L., B.M., and B.Z. researched, analyzed, interpreted data, and edited the manuscript. P.C., A.B., J.P., and H.N. researched and analyzed data and edited the manuscript. J.L. and J.E. analyzed and interpreted data and edited the manuscript. F.Y.F. and O.K. initiated the study, interpreted data, and edited the manuscript. O.E. initiated the study, researched, analyzed, interpreted data, and edited the manuscript. All co-authors read and approved the final version of the manuscript.

### DECLARATION OF INTERESTS

B.M. and O.E. are employees of Antaros Medical AB. F.Y.F. is an employee of Affibody AB. O.K. and O.E. are shareholders of Antaros Tracer AB.

Received: December 2, 2023

Revised: February 2, 2024

Accepted: April 5, 2024

Published: April 10, 2024

REFERENCES

- Wynn, T.A. (2004). Fibrotic disease and the TH1/TH2 paradigm. *Nat. Rev. Immunol.* 4, 583–594. <https://doi.org/10.1038/nri1412>.
- (2015). EASL-ALEH Clinical Practice Guidelines: Non-invasive tests for evaluation of liver disease severity and prognosis. *J. Hepatol.* 63, 237–264. <https://doi.org/10.1016/j.jhep.2015.04.006>.
- Patel, K., and Sebastiani, G. (2020). Limitations of non-invasive tests for assessment of liver fibrosis. *JHEP Rep.* 2, 100067. <https://doi.org/10.1016/j.jhepr.2020.100067>.
- Myers, R.P., Fong, A., and Shaheen, A.A.M. (2008). Utilization rates, complications and costs of percutaneous liver biopsy: a population-based study including 4275 biopsies. *Liver Int.* 28, 705–712. <https://doi.org/10.1111/j.1478-3231.2008.01691.x>.
- Pinzani, M., Milani, S., Herbst, H., DeFranco, R., Grappone, C., Gentilini, A., Caligiuri, A., Pellegrini, G., Ngo, D.V., Romanelli, R.G., and Gentilini, P. (1996). Expression of platelet-derived growth factor and its receptors in normal human liver and during active hepatic fibrogenesis. *Am. J. Pathol.* 148, 785–800.
- Wong, L., Yamasaki, G., Johnson, R.J., and Friedman, S.L. (1994). Induction of beta-platelet-derived growth factor receptor in rat hepatic lipocytes during cellular activation *in vivo* and in culture. *J. Clin. Invest.* 94, 1563–1569. <https://doi.org/10.1172/JCI117497>.
- Friedman, S.L., Roll, F.J., Boyles, J., and Bissell, D.M. (1985). Hepatic lipocytes: the principal collagen-producing cells of normal rat liver. *Proc. Natl. Acad. Sci. USA* 82, 8681–8685. <https://doi.org/10.1073/pnas.82.24.8681>.
- Wegrzyniak, O., Zhang, B., Rokka, J., Rosstedt, M., Mitran, B., Cheung, P., Puuvuori, E., Ingvast, S., Persson, J., Nordström, H., et al. (2023). Imaging of fibrogenesis in the liver by [(18)F]TZ-Z09591, an Affibody molecule targeting platelet derived growth factor receptor β. *EJNMMI Radiopharm. Chem.* 8, 23. <https://doi.org/10.1186/s41181-023-00210-6>.
- Cleeren, F., Lecina, J., Bridoux, J., Devoogdt, N., Tshibangu, T., Xavier, C., and Bormans, G. (2018). Direct fluorine-18 labeling of heat-sensitive biomolecules for positron emission tomography imaging using the Al(18)F-RESCA method. *Nat. Protoc.* 13, 2330–2347. <https://doi.org/10.1038/s41596-018-0040-7>.
- Keramida, G., Potts, J., Bush, J., Verma, S., Dizdarevic, S., and Peters, A.M. (2014). Accumulation of (18)F-FDG in the liver in hepatic steatosis. *AJR Am. J. Roentgenol.* 203, 643–648. <https://doi.org/10.2214/AJR.13.12147>.
- Ali, M.A., El-Abd, E., Morsi, M., El Safwany, M.M., and El-Sayed, M.Z. (2023). The effect of hepatic steatosis on 18F-FDG uptake in PET-CT examinations of cancer Egyptian patients. *Eur. J. Hybrid Imaging* 7, 19. <https://doi.org/10.1186/s41824-023-00173-6>.
- Shinzato, R.I.N., Nishie, A., Tamaki, T., Wada, N., Takatsuki, M., and Iida, G.Y.O. (2023). Prediction of Early-stage Liver Fibrosis Using FDG-PET/CT. *Anticancer Res.* 43, 4221–4227. <https://doi.org/10.21873/anticancer.16614>.
- Iredale, J.P., Benyon, R.C., Pickering, J., McCullen, M., Northrop, M., Pawley, S., Hovell, C., and Arthur, M.J. (1998). Mechanisms of spontaneous resolution of rat liver fibrosis. Hepatic stellate cell apoptosis and reduced hepatic expression of metalloproteinase inhibitors. *J. Clin. Invest.* 102, 538–549. <https://doi.org/10.1172/JCI1018>.
- Qin, X., Guo, X., Liu, T., Li, L., Zhou, N., Ma, X., Meng, X., Liu, J., Zhu, H., Jia, B., and Yang, Z. (2023). High *in-vivo* stability in preclinical and first-in-human experiments with [18F]AIF-RESCA-MIRC213: a 18F-labeled nanobody as PET radiotracer for diagnosis of HER2-positive cancers. *Eur. J. Nucl. Med. Mol. Imaging* 50, 302–313. <https://doi.org/10.1007/s00259-022-05967-7>.
- Liu, J., Guo, X., Wen, L., Wang, L., Liu, F., Song, G., Zhu, H., Zhou, N., and Yang, Z. (2023). Comparison of renal clearance of [18F] AIF-RESCA-HER2-BCH and [18F]AIF-NOTA-HER2-BCH in mice and breast cancer patients. *Eur. J. Nucl. Med. Mol. Imaging* 50, 2775–2786. <https://doi.org/10.1007/s00259-023-06232-1>.
- Buhl, E.M., Djudjaj, S., Babickova, J., Klinkhammer, B.M., Folestad, E., Borkham-Kamphorst, E., Weiskirchen, R., Hudkins, K., Alpers, C.E., Eriksson, U., et al. (2016). The role of PDGF-D in healthy and fibrotic kidneys. *Kidney Int.* 89, 848–861. <https://doi.org/10.1016/j.kint.2015.12.037>.
- Fellström, B., Klareskog, L., Heldin, C.H., Larsson, E., Rönstrand, L., Terracio, L., Tufveson, G., Wahlberg, J., and Rubin, K. (1989). Platelet-derived growth factor receptors in the kidney—Upregulated expression in inflammation. *Kidney Int.* 36, 1099–1102. <https://doi.org/10.1038/ki.1989.306>.
- Hudkins, K.L., Gilbertson, D.G., Carling, M., Taneda, S., Hughes, S.D., Holdren, M.S., Palmer, T.E., Topouzis, S., Haran, A.C., Feldhaus, A.L., and Alpers, C.E. (2004). Exogenous PDGF-D is a potent mesangial cell mitogen and causes a severe mesangial proliferative glomerulopathy. *J. Am. Soc. Nephrol.* 15, 286–298. <https://doi.org/10.1097/01.asn.0000108522.79652.63>.
- Kisseleva, T., Cong, M., Paik, Y., Scholten, D., Jiang, C., Benner, C., Iwaisako, K., Moore-Morris, T., Scott, B., Tsukamoto, H., et al. (2012). Myofibroblasts revert to an inactive phenotype during regression of liver fibrosis. *Proc. Natl. Acad. Sci. USA* 109, 9448–9453. <https://doi.org/10.1073/pnas.1201840109>.
- Krizhanovsky, V., Yon, M., Dickens, R.A., Hearn, S., Simon, J., Miething, C., Yee, H., Zender, L., and Lowe, S.W. (2008). Senescence of activated stellate cells limits liver fibrosis. *Cell* 134, 657–667. <https://doi.org/10.1016/j.cell.2008.06.049>.
- Wynn, T.A. (2007). Common and unique mechanisms regulate fibrosis in various fibroproliferative diseases. *J. Clin. Invest.* 117, 524–529. <https://doi.org/10.1172/JCI31487>.
- Zeisberg, M., and Kalluri, R. (2013). Cellular mechanisms of tissue fibrosis. 1. Common and organ-specific mechanisms associated with tissue fibrosis. *Am. J. Physiol. Cell Physiol.* 304, C216–C225. <https://doi.org/10.1152/ajpcell.00328.2012>.
- Klinkhammer, B.M., Floege, J., and Boor, P. (2018). PDGF in organ fibrosis. *Mol. Aspects Med.* 62, 44–62. <https://doi.org/10.1016/j.mam.2017.11.008>.
- (2018). Global, regional, and national incidence, prevalence, and years lived with disability for 354 diseases and injuries for 195 countries and territories, 1990–2017: a systematic analysis for the Global Burden of Disease Study 2017. *Lancet* 392, 1789–1858. [https://doi.org/10.1016/S0140-6736\(18\)32279-7](https://doi.org/10.1016/S0140-6736(18)32279-7).
- Younossi, Z.M., Golabi, P., Paik, J.M., Henry, A., Van Dongen, C., and Henry, L. (2023). The global epidemiology of nonalcoholic fatty liver disease (NAFLD) and nonalcoholic steatohepatitis (NASH): a systematic review. *Hepatology* 77, 1335–1347. <https://doi.org/10.1097/HEP.0000000000000004>.
- (2017). Worldwide trends in body-mass index, underweight, overweight, and obesity from 1975 to 2016: a pooled analysis of 2416 population-based measurement studies in 128.9 million children, adolescents, and adults. *Lancet* 390, 2627–2642. [https://doi.org/10.1016/S0140-6736\(17\)32129-3](https://doi.org/10.1016/S0140-6736(17)32129-3).
- Zhou, B., Lu, Y., Hajifathalian, K., Bentham, J., Di Cesare, M., Danaei, G., Bixby, H., Cowan, M.J., Ali, M.K., Taddei, C., et al. (2016). Worldwide trends in diabetes since 1980: a pooled analysis of 751 population-based studies with 4.4 million participants. *Lancet* 387, 1513–1530. [https://doi.org/10.1016/S0140-6736\(16\)00618-8](https://doi.org/10.1016/S0140-6736(16)00618-8).
- Younossi, Z.M., Tampi, R., Priyadarshini, M., Nader, F., Younossi, I.M., and Racila, A. (2019). Burden of Illness and Economic Model for Patients With Nonalcoholic Steatohepatitis in the United States. *Hepatology* 69, 564–572. <https://doi.org/10.1002/hep.30254>.
- Löfblom, J., Feldwisch, J., Tolmachev, V., Carlsson, J., Ståhl, S., and Frejd, F.Y. (2010). Affibody molecules: Engineered proteins for therapeutic, diagnostic and biotechnological applications. *FEBS Lett.* 584, 2670–2680. <https://doi.org/10.1016/j.febslet.2010.04.014>.
- Puuvuori, E., Chiodaroli, E., Estrada, S., Cheung, P., Lubenow, N., Sigfridsson, J., Romelin, H., Ingvast, S., Elgland, M., Liggieri, F., et al. (2023). PET Imaging of Neutrophil Elastase with (11)C-GW457427 in Acute Respiratory Distress Syndrome in Pigs. *J. Nucl. Med.* 64, 423–429. <https://doi.org/10.2967/jnumed.122.264306>.
- Selvaraju, R.K., Bulenga, T.N., Espes, D., Lubberink, M., Sörensen, J., Eriksson, B., Estrada, S., Velikyan, I., and Eriksson, O. (2015). Dosimetry of [(68)Ga]Ga-DO3A-VS-Cys(40)-Exendin-4 in rodents, pigs, non-human primates and human - repeated scanning in human is possible. *Am. J. Nucl. Med. Mol. Imaging* 5, 259–269.

## STAR★METHODS

## KEY RESOURCES TABLE

REAGENT or RESOURCE	SOURCE	IDENTIFIER
<b>Antibodies</b>		
Rabbit, monoclonal [Y92] anti- PDGFR $\beta$	Abcam	Cat#ab32570, RRID:AB_777165
<b>Chemicals, peptides, and recombinant proteins</b>		
RESCA-Z09591	this paper	N/A
<b>Experimental models: Cell lines</b>		
K-562 (female, <i>Homo sapiens</i> )	ATCC	Cat#CCL243
U-87 (male, <i>Homo sapiens</i> )	ATCC	Cat#HTB-14, RRID:CVCL_0022
<b>Experimental models: Organisms/strains</b>		
BALB/C mice (female)	TACONIC	Cat#BALB/cAnNTac, RRID:IMSR_TAC:BALB
BALB/C nu/nu mice (female)	TACONIC	Cat#C.Cg/AnNTac-Foxn1 <sup>nu</sup> NE9, RRID:IMSR_TAC:BALBNU
Sprague Dawley rats (male)	TACONIC	Cat#NTac:SD, RRID:RGD_1566440
Pig (male)	Local breeder	N/A
<b>Software and algorithms</b>		
GraphPad Prism 9.3.1	Dotmatics	RRID:SCR_002798
Pmod 4.0	PMOD Technologies	RRID:SCR_016547
ImageJ	ImageJ	RRID:SCR_003070
QuPath	QuPath	RRID:SCR_018257
<b>Other</b>		
nanoPET/MRI scanner	Mediso Medical Imaging Systems	N/A

## RESOURCE AVAILABILITY

## Lead contact

Further information and requests for resources and reagents should be directed to and will be fulfilled by the Lead Contact, Olof Eriksson ([olof.eriksson@ilk.uu.se](mailto:olof.eriksson@ilk.uu.se)).

## Materials availability

The reagent RESCA-Z09591 was generated during this study. Availability is restricted ,e.g. requiring a Material Transfer Agreement.

## Data and code availability

- Data: All data that support the findings of this study is available from the [lead contact](#) on reasonable request.
- Code: This paper does not report original code.
- Any additional information required to reanalyze the data reported in this work paper is available from the [lead contact](#) upon request.

## EXPERIMENTAL MODEL AND STUDY PARTICIPANT DETAILS

## Cell lines

Cell binding assays were conducted on PDGFR $\beta$ -expressing cells (U-87 human glioblastoma, male) (RRID:CVCL\_0022) and K-562 human (female) chronic myelogenous leukemia (PDGFR $\beta$ -negative cells) (RRID:CVCL\_0004) (both from ATCC, [Table S1](#)). The details of the cell lines can be found in the [key resources table](#). U-87 cells were cultured in Eagle's minimum essential medium (ATCC) and K562 cells in Roswell Park Memorial Institute (RPMI)-1640 medium (Biowest) with 10% fetal bovine serum (Merck, Germany) and 1% penicillin-Streptomycin (Biochrom, Berlin, Germany) at 37°C. The pellets of both cell lines were then frozen, embedded in optimal cutting temperature compound (OCT), and stored at -80°C. Frozen sections (20  $\mu$ m) were obtained using a cryostat microtome (Micron HM560, Germany), and mounted on Superfrost Plus microscope slides (Menzel-Gläser, Germany). Moreover, U-87 cells were suspended in PBS to be injected into mice for the xenograft model, as described in [method details](#).

### Human liver biopsy

A liver biopsy from a patient with liver fibrosis was obtained from the Uppsala Biobank (#827). The Swedish Ethical Review Authority (2019-02790) has approved the use of human biopsies in ARG-binding studies. The fibrotic stage of the biopsy used was determined to be severe (F3) by a blinded pathologist.

### Animal models

Two male Sprague Dawley rats (RRID:RGD\_1566440) were used for dosimetry ( $362.5 \pm 17.7$  g, 3 months old). U-87 xenografts were induced in female BALB/C nu/nu mice (RRID:IMSR\_TAC:BALBNU,  $19 \pm 1$  g, 3 months old) ( $n=10$ ). The mouse model for liver fibrosis was based on BALB/c (RRID:RGD\_1566440) female mice ( $22.8 \pm 1.6$  g, 3-4 months old) ( $n=51$ ). Mice and rats (from TACONIC) were housed at five and 2 respectively, per cage lined with bedding (GLP Aspen Bedding, TAPVEI). The animals had access to food and water *ad libitum*. They were maintained at a constant temperature of 22°C and humidity (50%) in a 12 h light/12 h dark rhythm. The pig (male, 2 months old and weighing 29kg) was acquired from a local breeder on the morning of the experiment. The Animal Ethics Committee of the Swedish Animal Welfare Agency has approved all experimental protocols (5.8.18-08564/2019, 5.8.18-06578/2019, and 5.8.18-15648/2019). The procedures were performed in agreement with the ARRIVE (Animal Research: Reporting of *In Vivo* Experiments) recommendations and institutional guidelines ("Uppsala University guidelines on animal experimentation", UFV 2007/724). See [method details](#) section for more information.

## METHOD DETAILS

### RESCA-Z09591 Affibody molecule production

A minimized version of the Affibody molecule Z09591 was synthesized using chemical solid-phase peptide synthesis (Almac). The Affibody molecule scaffold consists of 58 amino acids that form a tertiary structure of 3 alpha helices.<sup>29</sup> Thirteen residues are typically variable, and all of them are located on helices 1 and 2, which together form the binding surface. The remaining residues are constant, such as helix 3, which is necessary for maintaining high thermal stability and facilitating refolding. Here, the thirteen variable residues have been optimized to enhance the Affibody molecule's affinity for the extracellular domain of PDGFR $\beta$ . A unique cysteine was added at position 59 at the C-terminal to enable the facile functionalization of the construct. Next, a RESCA metal chelator was site specifically covalently conjugated to the cysteine via maleimide chemistry ((+)-H3RESCA-maleimide, Chematech). The final RESCA-Z09591 construct was purified and aliquoted into freeze-dried formulation in 100  $\mu$ g vials. Purity and identity were verified by high-performance liquid chromatography (HPLC) and mass spectrometry.

### Radiolabeling of RESCA-Z09591

Labeling of RESCA-Z09591 was conducted under metal-free conditions. The process began by trapping cyclotron-produced [<sup>18</sup>F]fluoride in a QMA cartridge (Sep-Pak Accell Plus QMA Plus light cartridge (Waters)). The cartridge was eluted with 200  $\mu$ L of saline, and then AlCl<sub>3</sub> in aqueous NaOAc was added to the solution and left to react at room temperature (rt) for 5 min. Subsequently, the solution containing [<sup>18</sup>F]AlF was mixed with RESCA-Z09591 and allowed to react for 12 min. The product solution was then loaded onto a NAP5 column and purified by elution with phosphate-buffered saline (PBS)/10% EtOH. Quality control of the eluate was performed by radio-HPLC (Agilent 1290 Infinity II system (Agilent Technologies)).<sup>9</sup>

To determine the optimal labeling conditions, several test reactions were performed to investigate the temperature, reagent ratios, and agitation requirements. From a starting activity of 1.1-1.5 GBq, the highest radiochemical yields (RCY) were achieved using 100  $\mu$ g RESCA-Z09591 in 100  $\mu$ L aqueous NaOAc and 6  $\mu$ L AlCl<sub>3</sub> solution at 60°C, without agitation. RCY in these conditions was approximately 30%. Moreover, the use of NAP5 columns in the purification step guaranteed a radiochemical purity (RCP) of >96%. Radiolabeling was tested at 37-60°C. A temperature of 60°C was ultimately selected because it was well-tolerated by the Affibody molecule Z09591 and resulted in overall high yields.

The detailed protocol for Al(18)F labeling of RESCA-conjugated Affibody molecules will be published separately.

### *In vitro* studies

#### Surface plasmon resonance studies

The affinities of RESCA-Z09591 to the recombinant human PDGFR  $-\beta$  and  $-\alpha$  (rhPDGFR $\beta$ , rhPDGFR $\alpha$ ), and recombinant murine PDGFR $\beta$  (rmPDGFR $\beta$ ) were analyzed using a Biacore® T200 surface plasmon resonance (SPR) instrument (GE Healthcare). The three target proteins were diluted to 10  $\mu$ g/ml in an acidic immobilization buffer consisting of 10 mM Acetate pH 5.0 for the human receptors and pH 4.5 for the murine receptor. rhPDGFR $\beta$ , rhPDGFR $\alpha$ , and rmPDGFR $\beta$  receptors were immobilized by amine coupling in separate flow cells of a CM-5 sensor chip (GE Healthcare). To reduce mass-transport limitations, the immobilization density was maintained low (400-600RU). The analyte, RESCA-Z09591, was diluted in hepes buffered saline (HBS-EP) buffer (10 mM HEPES, 0.15 mM NaCl, 3 mM EDTA, and 0.05% v/v Surfactant P20, pH 7.4). A multi-cycle kinetic method with a broad concentration range of 3000 nM, diluted in a series of three times to 0.15 nM was used to study the affinity of RESCA-Z09591 binding to proteins. This was sufficient to achieve saturation. The interaction between the sample and the target was broken after injection with a 30 s injection of 10 mM NaOH and 1 M NaCl. To allow the surface to stabilize, it was left in HBS-EP buffer flow for 480 s before the start of a new sample cycle. Each sample was injected at a constant flow rate of 30  $\mu$ L/min over the receptor surface for 60 s and was left to dissociate for 180 s.

### *In vitro* autoradiography

*In vitro* ARG was performed on the cell pellets and fibrotic human liver. Prior to starting the experiments, the sections were thawed to room temperature. They were then pre-incubated in 150 mL of a solution of PBS and 1% bovine serum albumin (BSA) at room temperature for 15 min. Optionally, to study the specificity of the radiotracer 2  $\mu$ M of unlabeled Cys-Z09591 was added to the previous solution (blocking condition). After 15 min, [ $^{18}$ F]AIF-RESCA-Z09591 was added to the solution at a concentration of 5 nM (approximately 0.1 MBq/mL), followed by incubation for 60 min. To remove the unbound radiotracer, the sections were washed twice in cold PBS/BSA 1%, once in PBS and dipped in MQ water. The sections were then dried at 9 37°C for 10 min. A set of calibration standards was created by adding 10  $\mu$ L of the incubation solution containing the radiotracer to absorbent paper. Both the slides and standards were exposed to a phosphor-imaging plate (BAS-MS, Fuji-film) overnight and scanned using a Phosphor Imager (Amersham Typhoon FLA 9500 Phosphor Imager, GE). The resulting images were analyzed using ImageJ software (National Institutes of Health, US). Paraffin-embedded biopsies from the same fibrotic liver were also obtained and prepared for correlative histology.

### *Histology and immunohistochemistry*

The remaining half of the liver or tumor, leg muscle, and spleen biopsies from mice were fixed in paraformaldehyde 4% for one day, dehydrated in 70% ethanol, and embedded in paraffin. The paraffin-embedded human fibrotic liver biopsy was prepared in a similar manner. The paraffin blocks were sectioned at a thickness of 4  $\mu$ m and stained with hematoxylin-eosin (H&E), SIR, and Masson's Trichrome (MT) at the local hospital pathology department (Uppsala University Hospital) according to standard methods. In order to assess the tissue expression of the target of interest, PDGFR $\beta$ , the sections were immunostained for PDGFR $\beta$  using the autostainer Link 48 and Envion FLEX High pH visualization system (Agilent). Before incubating the primary antibody, antigen retrieval was performed using PT-Linker (Dako) and High pH Target Retrieval Buffer. The recombinant anti-PDGFR $\beta$  antibody (RRID:AB\_777165, see details in Table S2) was incubated at a 1:300 dilution for 60 min. Horseradish peroxidase (HRP)-conjugated secondary antibodies were then used against the primary antibodies. The slides were counterstained with Mayer's hematoxylin using the Tissue Tek Prisma Plus automated slide stainer (Sakura). The sections were digitally imaged using the Nanozoomer S60 (Hamamatsu) at 20.0 $\times$  magnification, and the images were viewed using QuPath-0.2.3. The percentages of PDGFR $\beta$  expression in liver biopsies were assessed using ImageJ, and the same intensity threshold was applied to define positive staining in all fields of view.

### *Transmission electron microscopy*

Liver biopsies for transmission electron microscopy (TEM) imaging were taken from CCl<sub>4</sub> treated and healthy mice. Immediately after euthanasia, small ( $\approx$  1 mg) tissues biopsies were taken from the excised liver. Each biopsy was fixed in 2.5% glutaraldehyde with 1% paraformaldehyde in 0.1 M buffer. The fixed biopsies were then processed with 1% Osmium tetroxide and dehydrated in increasing concentrations of ethanol. After dehydration, the biopsies were embedded in epoxy resin and polymerized by heat. Sections (50 nm) were processed by an ultramicrotome, collected on grids, and treated by uranyl acetate and lead citrate for contrast. Sections were air-dried and then imaged using TEM (FEI Technai G2) at 80 kV.

### *In vivo* studies

#### *PET/CT and dosimetry in pig*

The healthy Swedish Landrace pig (male, 2 months old and weighing 29 kg) was transported to the preparation room on the day of the study. Anesthesia was initially induced by intramuscular administration of tiletamine-zolazepam (Boehringer Ingelheim). The animal was then intubated and ventilated, while anesthesia was maintained through a continuous intravenous infusion of ketamine at a dosage of 20 mg/kg/h (Ketaminol), fentanyl at 5 mg/kg/h (Pharmalink) and pancuronium at 0.24 mg/kg/h (Pavulon, Organon Teknika). Standard monitoring procedures were implemented as previously described.<sup>30</sup> An arterial catheter was inserted to measure arterial pressure and collect blood samples, while multiple intravenous catheters were placed for the infusion of anesthesia, administration of PET tracer, and CT contrast agent. When the animal's condition was stabilized, it was positioned in a supine posture on the bed of a PET/CT scanner (Discovery MI, 25 cm Field of View, GE Healthcare). Whole-body CT scans were acquired for anatomical co-registration (high dose), positioning, and attenuation correction. [ $^{18}$ F]AIF-RESCA-Z09591 was administered intravenously as a bolus (102.18 MBq, equivalent to approximately 1  $\mu$ g/kg of peptide) and subsequently followed by a saline chase. Simultaneously with the administration of the tracer, the acquisition of PET images was initiated. The examination of the pig was conducted utilizing a dynamic multi-bed protocol. First, a 15 minutes dynamic PET scan was performed over the heart to acquire first-pass blood kinetics. Then, sequential whole body passes were performed for up to 165 minutes to obtain the kinetics in all tissues in one experiment (5 bed positions; first 5 passes with 2 min/bed (total 50 minutes), then 4 passes with 5 min/bed (total 100 minutes)). Arterial blood samples were drawn 15, 60, 120, and 180 minutes after administration of [ $^{18}$ F]AIF-RESCA-Z09591, and analyzed for radioactivity concentration in whole blood and plasma by a gamma counter. Additionally, the stability of [ $^{18}$ F]AIF-RESCA-Z09591 in plasma was measured in the samples taken after 15 and 60 minutes (see supplemental information for details).

After the PET scan, a CT scan with contrast enhancement was acquired for improved soft-tissue delineation. After the scans, the pig was euthanized under deep anesthesia by intravenous KCl.

PET/CT images were analyzed using PMOD 4.0 (PMOD Technologies). Tissues were segmented on summed or individual PET frames using CT projects as support. Segmentations were applied to all PET frames to read out the dynamic uptake data and expressed as SUV.

Dynamic SUV data was used to calculate tissue residence times (PMOD) and the human-predicted dosimetry of [<sup>18</sup>F]AIF-RESCA-Z09591 (OLINDA) as described previously.<sup>31</sup>

The SUV is calculated by multiplying the ratio of tissue radioactivity concentration (Bq) by the volume of the tissue (mL), and the ratio of the body weight (g) and the administered dose (Bq) (1).

$$\text{SUV} = \frac{\text{Radioactivity concentration tissue}}{\text{Volumetissue}} \times \frac{\text{Weight body}}{\text{Radioactivity injected}} \quad (\text{Equation 1})$$

### *In vivo plasma stability assessment*

Arterial blood samples from the pig were collected at time points (T<sub>0</sub>) 0min, (T<sub>1</sub>) 15min and (T<sub>2</sub>) 1 h at (EOS). The plasma was extracted from the blood by centrifugation (3000xg 2min, 4°C) and it was mixed with ACN at a ratio of 1:1 (precipitation process). For samples T<sub>1</sub> and T<sub>2</sub>, the labelled mixture was incubated at 37°C followed by a last step of centrifugation (16000Xg, 2 min, 4°C). This last centrifugation was applied for all labelled samples and the supernatant was filtered through a 2X0.2 μm nylon membrane filter. An amount of 5μl of this prepared plasma was injected into HPLC for analysis.

The stability study was performed by an HPLC (VWR HITACHI) system, equipped with a manual injection loop (max sample volume injected 20ul), a UV detector (wavelength range:210-280nm), a Chromaster pump 5110, and a radio-detector probe FC-3300 NaI/PMT using an Eckert /Ziegler dynamic range module for low (100k CPM) and High selected activities (12M CPM).

The sample analysis is based on reverse phase column Vydac C4 214 MS Grace i.d. 5 mm (50 mm × 4.6 mm) using a gradient elution method. There were 2 mobile phases, Mobile phase A corresponding to 0.1% TFA in de-ionized water, and mobile phase B was 0.1% TFA in Acetonitrile (MeCN). Elution was carried out at a flow rate 1ml/min, using the following elution program: 0-10 min (10%-90% B) and 10-12min (90%-10%B). Under these conditions, the retention times of free <sup>18</sup>F and intact [<sup>18</sup>F]AIF-RESCA-Z09591 were in the range of 0.57-0.87 min and 4.54-4.61 min respectively. The software Agilent OpenLAB Chromaster EZChrome Edition was used for data acquisition and analysis.

### *PET/CT and dosimetry in rat*

Dynamic whole-body PET/CT scans were conducted on two male Sprague Dawley rats (362.5 ± 17.68 g). Each rat was anesthetized using 0.6L/min of 3% sevoflurane in a mixture of 50% oxygen and 50% medical air. The rats were positioned in a prone position on a heated bed set at 37°C within a preclinical PET/ magnetic resonance imaging (MRI) scanner (nanoPET, 3T field strength, 10 cm field of view, Mediso). The positioning process was assisted by a scout MRI scan (GRE MultiFOV scout). An intravenous catheter in the tail was used to administer [<sup>18</sup>F]AIF-RESCA-Z09591 (8.13 ± 0.73 MBq) as a bolus. Simultaneously, the scanner acquisition was initiated and continued for a duration of 137min. The PET protocol was designed to provide repeated whole-body passes of increasing duration (3 beds per pass; 1min, 3min, 5min, 2 × 10min, 3 × 30min). Following the scan, the rats were euthanized and whole-body CT images were acquired for anatomical co-registration (SE MultiFOV). The whole-body PET/CT images were visualized and analyzed using the PMOD software (PMOD Technologies). Tissues of interest were segmented on summarized PET images and CT projections, and the SUV<sub>mean</sub> was determined for each time point. The entire body was also segmented. Additionally, the predicted dosimetry of [<sup>18</sup>F]AIF-RESCA-Z09591 in humans was calculated, similar to the approach used for pigs.

### *U-87 xenograft mice model*

U-87 xenografts were induced in female BALB/C nu/nu mice (weight: 19 ± 1 g) (n=10) by the subcutaneous implementation of U-87 cells (2 × 10<sup>6</sup> cells/mouse) in the hind leg four to six weeks before the experiment to allow tumor growth. Mice were used for histological study, ex vivo biodistribution, and PET/MRI imaging (Figure S1A), see details below.

### *CCl<sub>4</sub> mice model of liver fibrosis*

Liver fibrosis was induced in BALB/c female mice (n=35) by CCl<sub>4</sub> (Sigma) treatment. The details of the different groups are presented in Figure S1B. The mice received intraperitoneal injections of CCl<sub>4</sub> (0.5 mg/g of body weight) in corn oil (1:4, v/v), three times a week for six weeks. They were closely monitored for 30 min after each CCl<sub>4</sub> injection and once per day to ensure their well-being. In this study, n=16 healthy mice were also included as the control group. Additionally, within the CCl<sub>4</sub>-treated mice group, two groups were kept for 1 week or 2 weeks CCl<sub>4</sub> post-treatment to let the liver regenerates (regression phase).

All mice were used for ex vivo ARGs and histological studies, and ex vivo biodistribution (see details below). A subset of animals was used for PET/CT scans (details provided below).

### *PET/MRI and PET/CT in mice*

In each group of the U-87 xenograft experiment, one mouse was injected as a bolus through an intravenous catheter in the tail with 6 MBq (equivalent to 5 μg peptide) of [<sup>18</sup>F]AIF-RESCA-Z09591 alone, while another mouse was co-injected with 1 mg/kg of Cys-Z09591. Each mouse was placed in a prone posture on the scanner bed, and anesthesia was maintained using a continuous supply of 3% sevoflurane in a mixture of 50/50% oxygen/ medical air (0.06L/min), and body temperature was maintained at 37°C by bed heating. Whole-body PET/MRI scans

(nanoPET/MRI scanner, Mediso Medical Imaging Systems) were performed from the time of injection until 45 min p-i. Following PET/MRI scanning, the mice were euthanized, and tissues were collected for histological analysis as described below.

In the liver fibrosis experiment, the mice were administered a bolus injection via an intravenous catheter in the tail with 2MBq (equivalent to 1.5  $\mu$ g peptide) of [ $^{18}$ F]AIF-RESCA-Z09591 alone, or co-administered with 1 mg/kg of Cys-Z09591. Within the experimental framework involving a one-week regression phase, the RCY was different, leading to the administration of 2MBq, equivalent to 0.75  $\mu$ g of peptide ([ $^{18}$ F]AIF-RESCA-Z09591), to the mice.

Four mice underwent follow-up PET/CT scans. The first *in vivo* scan was performed at the peak of the disease (6wks CCl<sub>4</sub>) and the second scan was conducted post-mortem at 1wk of regression (n=2) or 2wks of regression (n=2). The *in vivo* PET/CT scan was similar to the one performed on the xenograft. Except that the scan was static and lasted 20min and was followed by a 5min CT scan. In other conditions the PET/CT scans were conducted *post-mortem*. One hour, the mice were euthanized and a static whole-body PET/MRI scan (Mediso Medical ImagingSystems) was performed *post-mortem* to minimize movement artifacts. After the PET/MRI scans, the mice were dissected, and their organs were collected for *ex vivo* biodistribution and histological examination.

PET/MRI and PET/CT images were analyzed using PMOD 4.0 software (PMOD Technologies).

### Ex vivo biodistribution

Briefly, in the xenograft study, the mice were injected with either 0.6 MBq (equivalent to 0.5 $\mu$ g peptide) of [ $^{18}$ F]AIF-RESCA-Z09591 alone or co-injected with 1 mg/kg of Cys-Z09591 through an intravenous catheter in the tail. In the liver fibrosis experiment, CCl<sub>4</sub> mice and healthy mice were injected with 2 MBq (equivalent to 1.5 $\mu$ g peptide) of [ $^{18}$ F]AIF-RESCA-Z09591 alone, or co-injected with 1 mg/kg of Cys-Z09591. One hour post-injection the mice were euthanized, and blood was collected via heart puncture. The lungs, liver, spleen, kidneys, muscle, bone, (as well as the tumor for the U-87 xenograft mice) were harvested and weighed. Radioactivity uptake per organ was measured using a gamma counter, and decay was corrected at the time of injection. The tissue uptake measurement was corrected for decay and converted into SUVs.

### Ex vivo autoradiography

*Ex vivo* ARG was conducted on CCl<sub>4</sub> mice and healthy mice previously injected with [ $^{18}$ F]AIF-RESCA-Z09591 for the *ex vivo* biodistribution or PET/CT studies. Half of the liver, leg muscle, and spleen from the biodistribution study were snap-frozen and embedded in OCT. The OCT blocks were then sectioned into consecutive triplicates at a thickness of 20  $\mu$ m using a cryostat microtome (Micron HM560, Germany) and mounted on Superfrost Plus glass slides (Menzel-Gläser). Standards were created like the *in vitro* ARG. The slides and standards were exposed to a phosphor-imaging plate and scanned in a similar manner as *in vitro* ARG.

## QUANTIFICATION AND STATISTICAL ANALYSIS

Data are presented as mean  $\pm$  standard deviation (SD). "n" represent the number of cell pellets analyzed on the ARG results for Figures 2D and 2E, and the number of animals in all other figures. Normality was assessed using a Shapiro-Wilk test, and equality of variance was checked using an F-test. Data were analyzed using unpaired two-tailed Student's t-tests with or without Welch's correction or two-way analysis of variance (ANOVA) with Tukey's post-hoc tests. A significance level of 0.05 was used for all comparisons and \*\*  $p \leq 0.01$ , \*\*\*  $p \leq 0.001$ , \*\*\*\*  $p \leq 0.0001$ . GraphPad Prism 9.3.1 software (GraphPad Software, San Diego, CA, USA) was used to conduct statistical analyses. All statistical details of experiments can be found in the figure legends associated and supplementary data (Tables S7–S11).